JOURNAL OF COMPUTATIONAL PHYSICS 108, 199–208 (1993)

Numerical Conformal Mapping Methods for Exterior Regions with Corners

THOMAS K. DELILLO* AND ALAN R. ELCRAT†

Department of Mathematics and Statistics, Wichita State University, Wichita, Kansas 67260-0033

Received September 12, 1991; revised July 13, 1992

The main purpose of this paper is to present a method for computing the conformal map between the exterior of the unit disk and the exterior of a simple closed curve with corners. The method may be regarded as a generalization of the Schwarz–Christoffel transformation and is derived from the integral equation of Timman. Some comparison is made with other methods such as a version of Timman's equation with corners, Fornberg's method with explicit corner removers, Davis' method, and CONFPACK. The method proves to be quite flexible and robust.

I. INTRODUCTION

Various methods have been proposed for computing the conformal map between the unit disk and a simple closed curve with a finite number of corners; see [2, 5, 9–11, 14, 16, 20, 22]. For polygonal regions an efficient implementation of the Schwarz–Christoffel method is available [21]; see also [8, 12, 13]. Our main purpose here is to consider a method for mapping curvilinear polygons. The method may be considered as a generalization of the Schwarz–Christoffel transformation. Such generalizations have been suggested elsewhere; see [2, 3, 5, 9, 14, 20, 22]. However, we believe the approach and computations reported here are new and of interest.

Our method may be derived from the Timman method [4, 8], a method for mapping from the disk to regions with smooth boundaries. A version of Timman's method which allows corners to be included as Schwarz–Christoffel factors and uses FFTs has been suggested in [14, 16]. We discuss this method in Section II below and find it to be of only limited usefulness. In Section III, we discuss our new method. An integral equation for the boundary correspondence for the map from the region to the disk is derived from the Timman equation by integrating the Hilbert transform by parts as suggested in [3, 18], interchanging the dependent and independent variables and incorporating corners as jumps in the tangent angle. We will refer to this method henceforth as the "inverse Timman" method. The discretization of the equation, its solution by a method of successive approximation, and its accuracy are discussed. The method proves to be quite flexible and robust, although not as accurate near the corners as might be desired. Some suggestions are made for possibly improving the accuracy. In Section IV, some discussion and comparison is made with other methods. Combining explicit corner removers with FFT methods is an option; see [4, 7, 16]. We give an example of this procedure using Fornberg's method [6, 8]. Other generalizations of the Schwarz–Christoffel transformation such as [2, 9] are remarked on. Also, some comments are made on CONFPACK [11], a package based on solving Symm's integral equation with Jacobi polynomials [10]. In the remainder of this section we define our notation and explain how our boundary curves are parametrized.

Below, we will let g be the map from the exterior of the unit circle to the exterior of a simple closed curve $z = z(\sigma)$ parametrized by arc length $0 \leqslant \sigma \leqslant L$ and smooth, except at a finite number of corners at σ_k's. Then $g(e^{i\theta}) = z(\sigma(\theta))$, $g^{-1}(z(\sigma)) = e^{i\theta(\sigma)}$, and $\sigma_k = \sigma(\theta_k)$. K will denote the conjugation operator relating conjugate harmonic functions. The angle measured inside the (exterior) region at the kth corner is $\alpha_k \pi$, $\beta_k = \alpha_k - 1$; $\lambda(\sigma) = \arg z'(\sigma)$ and $g'(\infty) = \gamma e^{i\delta}$; g has the Laurent series expansion

$$g(w) = cw + a_0 + a_1 w^{-1} + \cdots,$$

where $c = g'(\infty) = \gamma e^{i\delta}$. The maps g here all have the normalization $g(\infty) = \infty$ and $g(1)$ fixed on the boundary.

The piecewise smooth curves which bound the regions that we deal with are given by spline curves, parameterized by chordal arc length on each smooth part; the tangents are specified at the end points of these arcs. Our program takes as data a set of points on each arc and the tangent directions

* Partially supported by a summer research fellowship from the Wichita State University College of Liberal Arts and Sciences, U.S. Department of Energy Grant DE-FG02-92ER25124, and National Science Foundation EPSCoR Grant OSR-9255223.

† Partially supported by U.S. Air Force Grant AFOSR89-0323 and National Science Foundation EPSCoR Grant OSR-9255223.

0021-9991/93 $5.00

at the end points. For most of the examples that we discuss these are generated by another program using analytic formulas which describe the smooth arcs to generate the points to be interpolated. In particular, it should be noted that in the case of smooth regions such as the ellipse the analyticity of the boundary is not used. A modification could be made to employ analytic parametrization, but σ would no longer be the arc length, in general.

II. TIMMAN'S METHOD WITH CORNERS

Aspects of this method are discussed in [1, 14, 16]. To derive the method we consider the auxiliary function, $h(w) = i \log((g'(w)/g'(\infty)) \prod_k (1 - w_k/w)^{-\beta_k})$ which is analytic for $|w| > 1$. Applying the conjugation relation between the real and imaginary parts of h,

$$\operatorname{Re} h(e^{i\theta}) - \operatorname{Re} h(\infty) = K[\operatorname{Im} h(e^{i\theta})],$$

and noting that

$$g'(e^{i\theta}) = -i\, e^{i\theta} \sigma'(\theta)\, z'(\sigma(\theta)),$$

$$1 - e^{i(\sigma_k - \sigma)} = 2 \sin\left(\frac{\sigma_k - \sigma}{2}\right) \exp(i(\sigma_k - \sigma - \pi)/2),$$

and $|z'(\sigma(\theta))| = 1$ yields

$$\log \sigma'(\theta) - \log \gamma + \sum_k \beta_k \log \left| 2 \sin\left(\frac{\sigma_k - \sigma}{2}\right)\right| = K\left[\lambda_s(\sigma(\theta)) - \left(1 + \frac{1}{2}\sum_k \beta_k\right)\theta\right].$$

Here

$$\lambda_s(\sigma(\theta)) = \lambda(\sigma(\theta)) - \pi \sum_k \beta_k H(\sigma - \sigma_k)$$

$$= \lambda(\sigma(\theta)) - \pi \sum_k \beta_k H(\theta - \theta_k)$$

is the tangent angle with the jumps subtracted and H is the Heaviside function.

A method of successive approximation is used, as with Timman's method; see [4, 8, 14]: the nth iterate $\sigma^n(\theta)$ is substituted for $\sigma(\theta)$ above. K is computed with N-point FFTs and an interpolation is done at each step to find the θ_k's for the corners. $\sigma'(\theta)$ is integrated at each iteration step to produce $\tilde{\sigma}^{n+1}(\theta)$. This is done by subtracting out the known singular contributions from the corners and treating them exactly. Finally, underrelaxation $\sigma^{n+1}(\theta) = \omega\, \tilde{\sigma}^{n+1}(\theta) + (1 - \omega)\, \sigma^n(\theta)$ is used, usually with $\omega = 0.5$, to produce the $(n+1)$th iterate. Convergence is linear. For smooth regions such as the ellipse and the inverted ellipse, Figs. 4 and 7, the error in the successive iterates decreased rapidly to roughly 10^{-6} in 20 iterations. The discretization error could be decreased to about 10^{-5}, as small as one would expect with our spline approximations to the analytic curves. The inverted ellipse is a difficult case for Fourier series methods and in this case the results were poor for $\alpha = 0.4$ and $N = 512$.

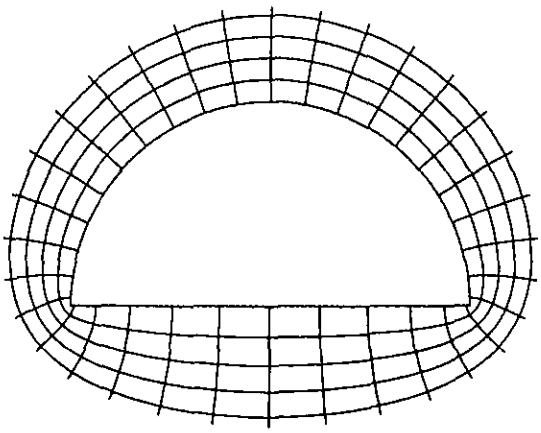

FIG. 1. Semicircle using Timman's method with corners, with $N = 256$ and $NP = 512$.

For regions with corners the results were disappointing. For the semicircle, Fig. 1, the cosine airfoil, Fig. 2, the equilateral triangle, Fig. 13, the square, Fig. 14, and the overlapping circles with $\psi_1 = 2.5$ and $\psi_2 = 2.7$, Fig. 8, the successive iteration error converged to 10^{-2} or 10^{-3} in several iterations for a range of N. Note that the corners for all these regions had $\alpha_k \pi > \pi$. For other regions in this paper, the overlapping circles with $\psi_1 = 0.9$ and $\psi_2 = 0.7$, Fig. 10, the wing-body, Fig. 11, and the thick wing-body, Fig. 18, which all have corners with $\alpha_k \pi < \pi$, the method failed to converge even with large N and underrelaxation by 0.05. Also the method failed for the quadrilateral, Fig. 15, and the flat plate, Fig. 5.

In the cases where the method works, it is fast, due to the use of FFTs. However, since linear interpolation is used at each step to compute the θ_k's the discretization error is roughly $O(N^{-1})$ and two or three place accuracy is probably all that can be expected. (Ives [16, p. 121] recommends this method over removing corners, but as we remark in Section IV below, corner removers may be somewhat more accurate.)

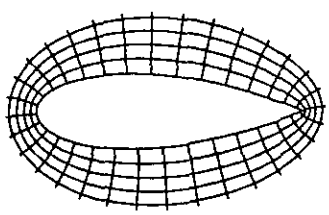

FIG. 2. Cosine airfoil using Timman's method with corners, with $N = 64$ and $NP = 128$.

III. THE INVERSE TIMMAN METHOD

The method in the previous section approximates the boundary correspondence $\sigma = \sigma(\theta)$ for the map from the disk to the region along with the preimages of the corners, θ_k. In this section we will investigate a new method for approximating the inverse boundary correspondence $\theta = \theta(\sigma)$ for the map from the region to the disk. The method may be regarded as a generalization of the Schwarz–Christoffel transformation. The relations between the equation given below and the equations of Timman and Davis [2] is given in [3]. Similar ideas are suggested in [5, 20, 22].

To derive our method we begin with the auxiliary function

$$h(w) = \log g'(w).$$

For h analytic for $|w| > 1$ the conjugation relation

$$\operatorname{Re} h(e^{i\theta}) - \operatorname{Re} h(\infty) = K[\operatorname{Im} h(e^{i\theta})]$$

gives Timman's equation

$$\log \sigma'(\theta) - \log \gamma = K[\lambda(\sigma(\theta)) - \theta - \pi/2].$$

Next we use the representation of the Hilbert transform K as a principal value integral which we integrate by parts (we note here that the Menikoff–Zemach equation [18] for $\theta = \theta(\sigma)$ is derived in a similar way starting with the auxiliary function, $h(w) = \log g(w)/w$, for the Theodorsen equation)

$$\begin{aligned}
\log \sigma'(\theta) - \log \gamma &= K[\lambda(\sigma(\theta)) - \theta] \\
&= \frac{1}{2\pi} PV \int_0^{2\pi} \cot\left(\frac{\theta - \tilde{\theta}}{2}\right) (\lambda(\sigma(\tilde{\theta})) - \tilde{\theta})\, d\tilde{\theta} \\
&= \frac{1}{\pi} \int_0^{2\pi} \log \left|\sin \frac{\theta - \tilde{\theta}}{2}\right| d(\lambda(\sigma(\tilde{\theta})) - \tilde{\theta}) \\
&= -\frac{1}{\pi} \int_0^{2\pi} \log \left|\sin \frac{\theta - \tilde{\theta}}{2}\right| d\tilde{\theta} \\
&\quad + \frac{1}{\pi} \int_0^{2\pi} \log \left|\sin \frac{\theta - \tilde{\theta}}{2}\right| d\lambda(\sigma(\tilde{\theta})).
\end{aligned}$$

Using the fact that the first integral in the last line above is equal to $\log 4$ and exchanging the dependent and independent variables σ and θ with $\sigma'(\theta) = 1/\theta'(\sigma)$ we obtain an equation for $\theta = \theta(\sigma)$,

$$\begin{aligned}
\log \theta'(\sigma) = &-\log \gamma - \log 4 \\
&- \frac{1}{\pi} \int_0^L \log \left|\sin \frac{\theta(\sigma) - \theta(\tilde{\sigma})}{2}\right| d\lambda(\tilde{\sigma}).
\end{aligned}$$

Using λ_s as in Section II and letting $\kappa(\sigma) = \lambda_s'(\sigma)$, the curvature on the smooth sections, we have the equation for $\theta(\sigma)$ which incorporates the β_k's at the corners,

$$\begin{aligned}
\log \theta'(\sigma) = &-\log 4 - \log \gamma - \sum_k \beta_k \log \left|\sin \frac{\theta(\sigma) - \theta_k}{2}\right| \\
&- \frac{1}{\pi} \int_0^L \log \left|\sin \frac{\theta(\sigma) - \theta(\tilde{\sigma})}{2}\right| \kappa(\tilde{\sigma})\, d\tilde{\sigma}
\end{aligned}$$

or

$$\begin{aligned}
\frac{d\theta}{d\sigma} = &\frac{1}{4\gamma} \prod_k \left|\sin \frac{\theta(\sigma) - \theta_k}{2}\right|^{-\beta_k} \\
&\times \exp\left(-\frac{1}{\pi} \int_0^L \log \left|\sin \frac{\theta(\sigma) - \theta(\tilde{\sigma})}{2}\right| \kappa(\tilde{\sigma})\, d\tilde{\sigma} \right).
\end{aligned}$$

This equation will be solved by a method of successive approximation. There are two integrations to perform: the "outer" integration of $d\theta/d\sigma$ between the mesh points and the "inner" integration from 0 to L in the exponential on the right side of the equation above. For the inner integration, we have found it helpful to subtract the logarithmic singularities as

$$\begin{aligned}
&\int_0^L \log \left|\sin \frac{\theta(\sigma) - \theta(\tilde{\sigma})}{2}\right| \kappa(\tilde{\sigma})\, d\tilde{\sigma} \\
&\quad = \int_0^L \log \left|\frac{\sin((\theta(\sigma) - \theta(\tilde{\sigma}))/2)}{\sigma - \tilde{\sigma}}\right| \kappa(\tilde{\sigma})\, d\tilde{\sigma} \\
&\qquad + \int_0^L \log|\sigma - \tilde{\sigma}|\, (\kappa(\tilde{\sigma}) - \kappa(\sigma))\, d\tilde{\sigma} \\
&\qquad + \kappa(\sigma) \int_0^L \log|\sigma - \tilde{\sigma}|\, d\tilde{\sigma}.
\end{aligned}$$

The last term can be integrated explicitly and the other two terms on the right side are smooth enough for our discretization to give sufficient accuracy. (We remark that there are other singularities in the integrand above, for instance, when $\sigma = 0$ and $\tilde{\sigma} = L$, but these are handled in a similar fashion.) The integrals can then be approximated by dividing each interval corresponding to a smooth arc into a number of subintervals and replacing the integral over each of the smaller subintervals with three-point Gaussian quadrature. The set of nodal points for all of these quadratures, together with the corner points, then serves as the mesh points for the computation. We denote these mesh points as σ_j, $j = 1, \ldots, M$. We have implemented a distribution in which the Gauss points lie on intervals equally spaced with respect to the maximum of arc length and the magnitude of the curvature, so that more mesh points are always distributed in regions of high curvature. Thus, for instance,

the first integral in the inner integration is replaced by a sum of the form

$$\sum_{j=1}^{M} \log \left| \frac{\sin((\theta(\sigma)-\theta(\sigma_j))/2)}{\sigma-\sigma_j} \right| w_j,$$

where the weights w_j depend on κ and the Gauss weights.

At each iteration we must integrate the approximation to $(d\theta/d\sigma)(\sigma)$ from σ_j to σ_{j+1}. In order to approximate this outer integral we need values of $(d\theta/d\sigma)(\sigma)$ at arbitrary σ such that $\sigma_j < \sigma < \sigma_{j+1}$. Hence, we need to interpolate the $\theta_j = \theta(\sigma_j)$, $j = 1, ..., M$, at each iteration. For this, since $\theta = \theta(\sigma)$ is monotonically increasing, we use the monotonicity-preserving Hermite cubic E01BEF from the NAG library. We have found that a simple midpoint rule works best for the outer integration. Thus, our nth iteration is of the form

$$\theta^{n+1}(\sigma_{j+1}) = \theta^{n+1}(\sigma_j) + \int_{\sigma_j}^{\sigma_{j+1}} \frac{d\theta^n}{d\sigma}(\tilde{\sigma})\, d\tilde{\sigma}$$

$$= \theta^{n+1}(\sigma_j) + (\sigma_{j+1}-\sigma_j)\frac{d\theta^n}{d\sigma}\left(\frac{\sigma_{j+1}+\sigma_j}{2}\right).$$

The $\theta^n(\sigma_j)$'s are normalized at each step so that $\theta^n(L) = 2\pi$. We note that the cost of each iteration is $O(M^2)$ and that the integrations from σ_j to σ_{j+1} could be done in parallel. We have tried more sophisticated methods than the midpoint rule for the outer integration such as Gauss–Jacobi, NAGLIB routines, charge-of-variables, adaptive eight-panel Newton–Cotes, adaptive quadrature, and mesh refinement near the corners, but they helped only slightly, if at all. Our computational experience suggests that the more sophisticated routines worked much harder to accurately compute integrals which were themselves inaccurate due, for instance, to the inherent error in approximating $\theta(\sigma)$ by a Hermite cubic. One possibility for improving the accuracy might be to replace the Hermite cubic by an interpolant which has the known singular behavior of $\theta(\sigma)$ at the corners. We have chosen not to pursue this possibility further here. We also note that the calculation of the curvature κ involves second derivatives of the cubic spline fit to the boundary curve $z = z(\sigma)$, so it may not be highly accurate.

The method always converges, in that the successive iteration error always goes to zero. This is even the case when the resulting approximation to the map is very poor, which may be disturbing. We have seen no "convergence/divergence" phenomenon, as was sometimes seen with Wegmann's method in [4]. These observations indicate that the discrete equations always have a solution. The con-

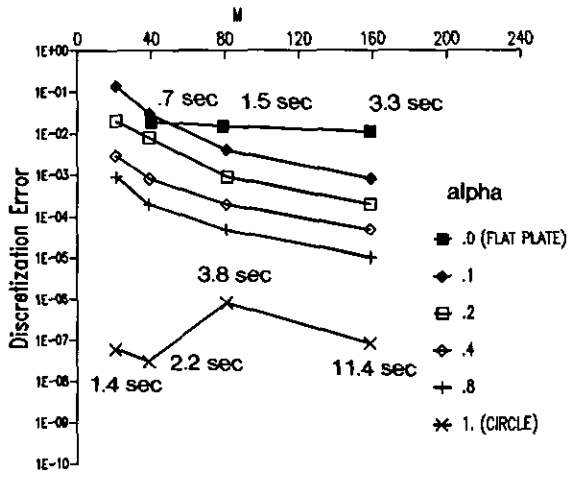

FIG. 3. Discretization error $\max|\theta - \theta_M|$, for the ellipse using the inverse Timman method.

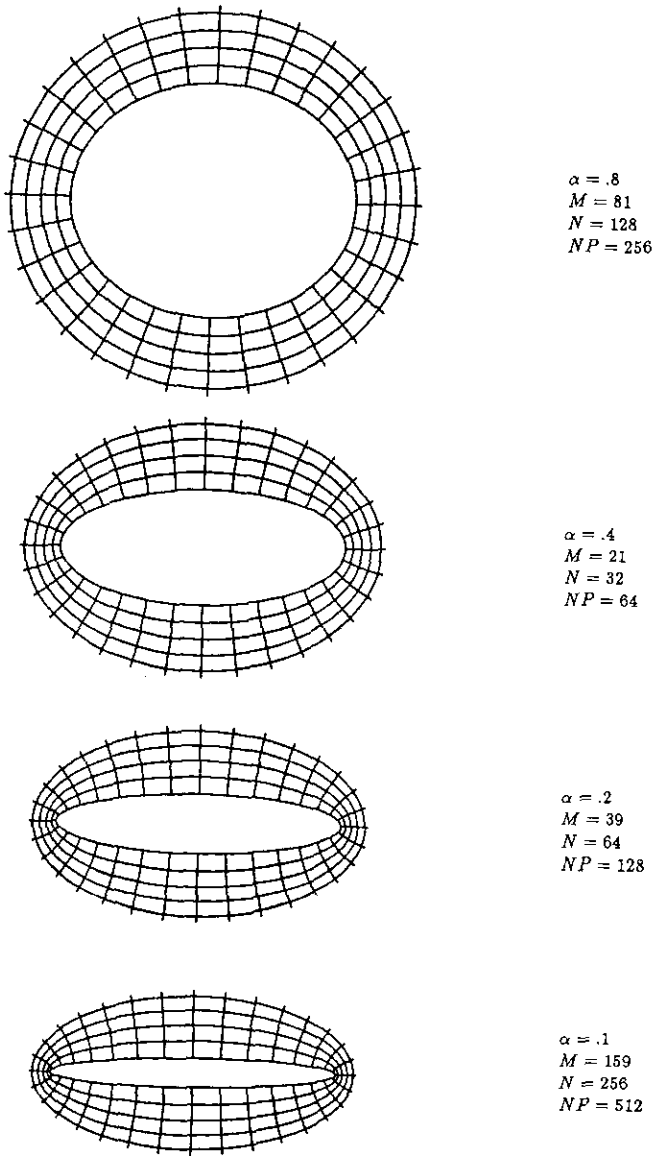

FIG. 4. Ellipses using the inverse Timman method.

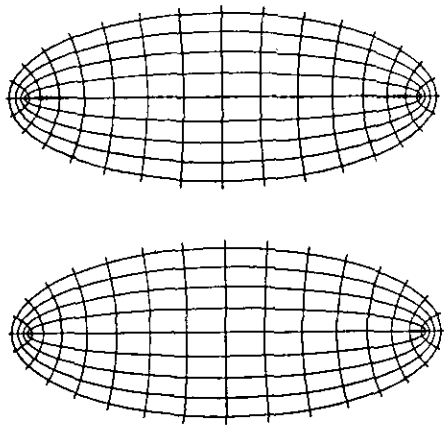

FIG. 5. Flat plate using the inverse Timman method with $M=40$, $N=128$, $NP=256$, $\max|\theta-\theta_M|=0.19\times10^{-1}$ (top); $M=159$, $N=256$, $NP=512$, $\max|\theta-\theta_M|=0.11\times10^{-1}$ (bottom).

vergence rate is linear with a factor of about $\frac{1}{3}$ to $\frac{1}{2}$ for most regions. Thus the successive iteration error is usually about 10^{-6} to 10^{-10} after 20 iterations. Underrelaxation by a factor of 0.7 always appears to be best. We presently have no convergence theory. The interested reader is referred to Kaiser's thesis [17] for convergence proofs for the related method of Timman.

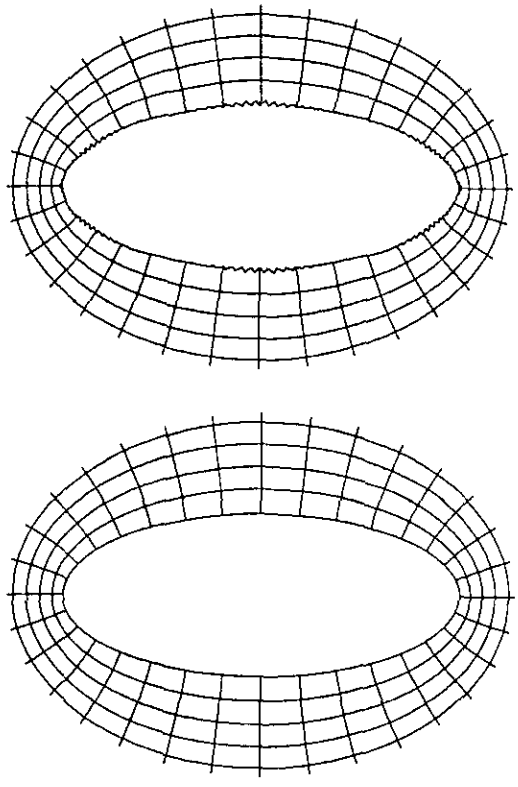

FIG. 6. For the ellipse with $\alpha=0.4$ inaccuracies in $\theta=\theta_M(\sigma)$ cause oscillations. For the top figure $M=39$, $N=128$, $NP=256$, and after one iteration $\max|\theta-\theta_M|=0.29\times10^{-1}$. For the bottom figure $M=39$, $N=128$, $NP=256$, and after several iterations $\max|\theta-\theta_M|=0.7\times10^{-3}$.

Before we present our examples, we make some general remarks on the effectiveness and accuracy of the method. The method is quite robust and reasonably fast. We can treat a wider class of both smooth curves and curves with corners than we could with either the Fourier series methods reported on in [4] or with Timman's method with corners in Section II above. The method shares the robustness of all methods which compute the map to the disk, thus avoiding the severe ill-conditioning due to the crowding phenomenon which can especially afflict maps to the region; see [4, 11–13, 18]. Accuracy away from the corners is usually acceptible (10^{-3} to 10^{-5}) with a few hundered mesh points. Accuracy near the corners may be low (10^{-1} to 10^{-2}). Improving the accuracy, especially at the corners, would probably require a better interpolant than the Hermite cubic as mentioned above, perhaps a piecewise Hermite cubic with correct behavior at the corners.

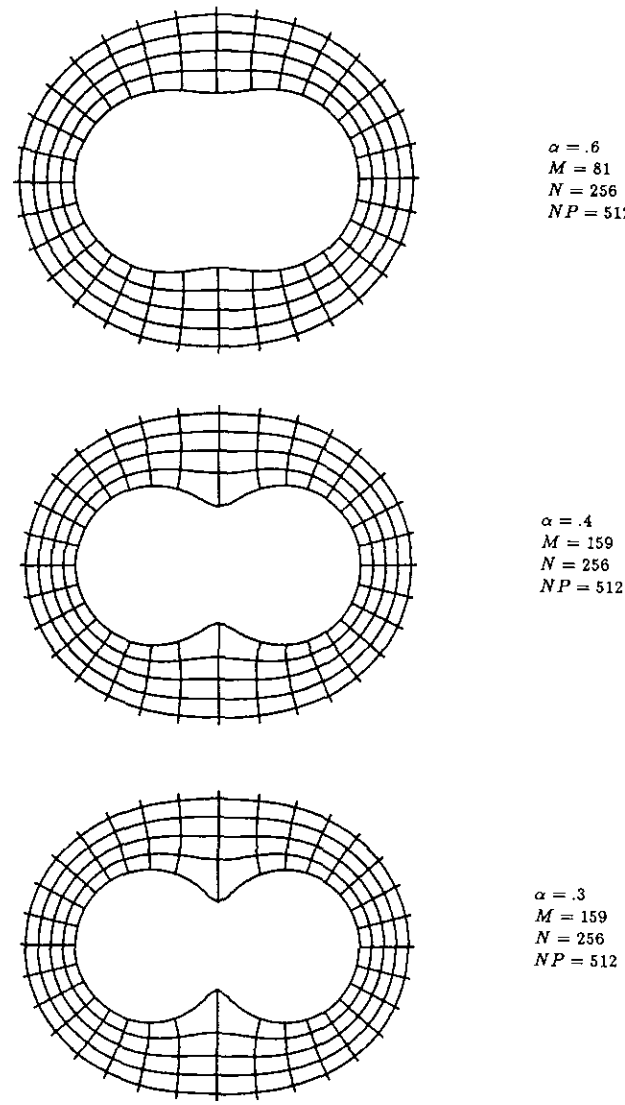

FIG. 7. Inverted ellipses using the inverse Timman method.

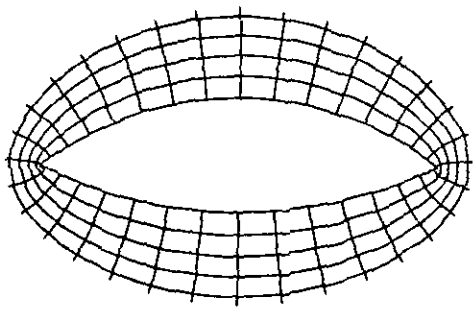

FIG. 8. Overlapping circles with $\psi_1 = 2.5$, $\psi_2 = 2.7$, $M = 58$, $N = 64$, $NP = 128$ using the inverse Timman method.

In order to plot the images of concentric circles and radial lines for the figures, we generate the Laurent series of g. This is computed by inverting the boundary correspondence $\theta_j = \theta(\sigma_j)$ to obtain $\sigma_j = \sigma(\theta_j)$, $j = 1, ..., M$, and then interpolating $\sigma_j = \sigma(\theta_j)$ with the monotonicity preserving Hermite cubic E01BEF. The images of N Fourier points $z_i = z(\sigma(\theta_i))$, $\theta_i = 2\pi i/N$, $i = 0, 1, ..., N-1$, can then be evaluated and an N-point Fourier (Laurent) series approximation to g can then be generated with an FFT. We plot $NP > N$ images of Fourier points on the concentric circles. In most cases discretization errors in $\sigma = \sigma(\theta)$ at the Fourier points were about the same as the errors in $\theta = \theta(\sigma)$ at the mesh points.

The rounded acute corners, seen in the figures for the wing-body, overlapping circles, or notched circles, are artifacts of the Fourier series approximation to g. The computational "proof" of this is that the same rounding is seen when the Laurent series is generated with the exact map. The oscillations occasionally seen on the boundary are the result of inaccuracies in $\theta = \theta(\sigma)$. The computational "proof" of this is shown in Fig. 6 with the ellipse $\alpha = 0.4$ and $M = 39$, where the results of only one iteration are compared to the converged solution.

EXAMPLE a (Ellipse, Fig. 4). The curve is given by

$$z(\tau) = \alpha e^{i\tau}/\sqrt{1-(1-\alpha^2)\cos^2\tau}, \qquad 0 \leqslant \tau \leqslant 2\pi,$$

where $0 < \alpha \leqslant 1$. The exact boundary correspondence is

$$\theta(\tau) = \arctan(\alpha^{-1}\tan\tau).$$

The exact map, including the "flat plate" case $\alpha = 0$, is known. Discretization errors for the new method are given Fig. 3. For comparison of this case with Fourier series methods see [4]. Note again that we do not use the analyticity of the boundary in our computations. The computations were done on an IBM ES9000 Model 440 and some timings are given next to the data points. (The timings in [4] were for an IBM 3081 and should be divided by a factor of about 3 for comparison. The timings reported here for the IBM ES9000 did not make use of the vectorizing capabilities.)

EXAMPLE b (Inverted ellipse, Fig. 7). This curve is given by

$$z(\tau) = \sqrt{1-(1-\alpha^2)\sin^2\tau}\, e^{i\tau}, \qquad 0 \leqslant \tau \leqslant 2\pi,$$

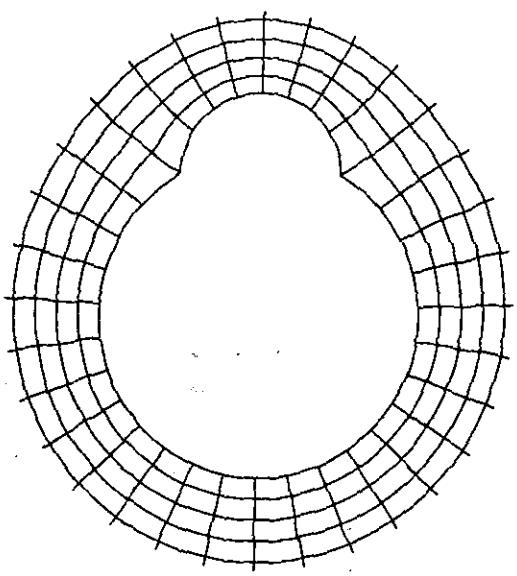

FIG. 9. Overlapping circles with $\psi_1 = \pi/2$, $\psi_2 = \pi/6$, $M = 199$, $N = 256$, $NP = 512$ using the inverse Timman method (see Table I).

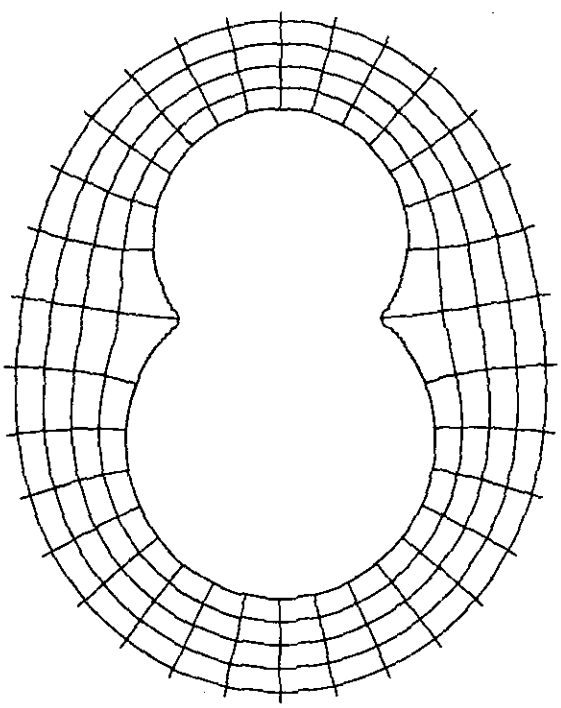

FIG. 10. Overlapping circles with $\psi_1 = 0.9$, $\psi_2 = 0.7$, $M = 150$, $N = 512$, $NP = 2048$ using the inverse Timman method.

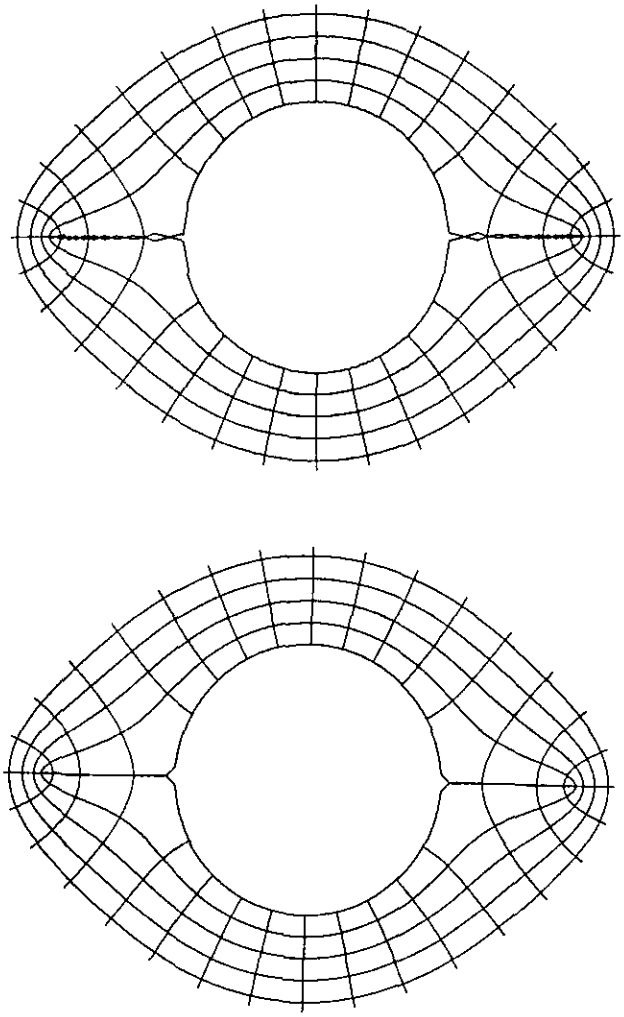

FIG. 11. The wind-body using the inverse Timman method with $M = 104$, $N = 128$, $NP = 256$ (top) and $M = 296$, $N = 512$, $NP = 1024$ (bottom).

TABLE I

Discretization Error for Overlapping Circles with $\psi_1 = \pi/2$ and $\psi_2 = \pi/6$ Using the Inverse Timman Method (See Fig. 9)

M	$\lvert\theta - \theta_M\rvert$	N	$\lvert\sigma - \sigma_N\rvert$	$\lvert 1 - \lvert f(z)\rvert\ \rvert$	CPU seconds (IBM ES9000)
49	0.11×10^{-1}	512	0.50×10^{-1}	0.13×10^{-1}	0.9
97	0.48×10^{-2}	512	0.21×10^{-1}	0.63×10^{-2}	3.8
199	0.22×10^{-2}	512	0.11×10^{-1}	0.36×10^{-2}	15.6
301	0.15×10^{-2}	512	0.94×10^{-2}	0.20×10^{-2}	28.0

where $0 < \alpha \leqslant 1$. Again, comparison can be made with the Fourier series methods in [4]. For small α this is a difficult mapping problem due to the severe crowding near the "fingering" sections. Our method with $\alpha = 0.3$ required $M = 160$, whereas Wegmann's method in [4] required $N = 2048$.

EXAMPLE c (Overlapping circles, Figs. 8–10). The exact map in this case is given in [15], essentially by mapping the region to a wedge and removing the corners. In our case the figures are symmetric about the x and y axes. ψ_1 is the angle between the x-axis and the upper circle and ψ_2 is the angle between the x-axis and the lower circle. Discretization errors are give in Table I for $\psi_1 = \pi/2$ and $\psi_2 = \pi/6$.

In this example and the next we compute an estimate of the error in $f = g^{-1}$, $\max \lvert 1 - \lvert f(z)\rvert\ \rvert$ for z on the boundary. To do this, we use the fact that $(1/2\pi)\,\theta'(\sigma)$ is the solution to Symm's equation for the exterior problem; see [8, 10, or 11]. We then have

$$f(z) = \gamma^{-1} e^{(i\omega + P(z))},$$

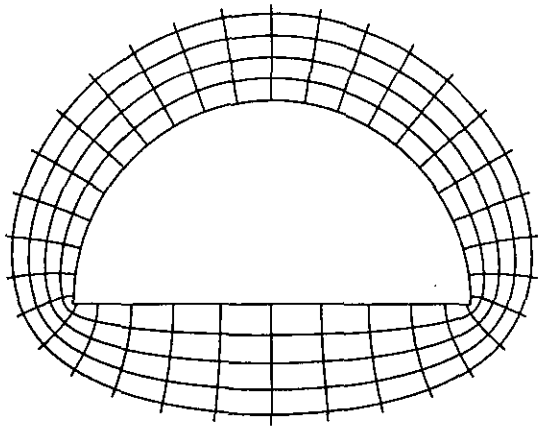

FIG. 12. Semicircle using the inverse Timman method with $M = 196$, $N = 512$, $NP = 2048$.

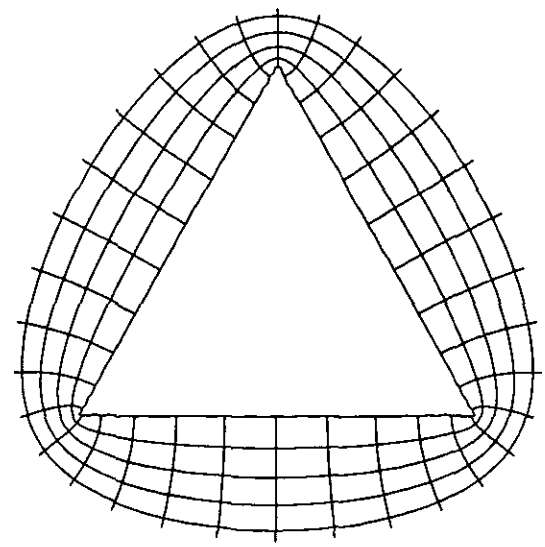

FIG. 13. Triangle using the inverse Timman method with $M = 59$, $N = 64$, $NP = 128$.

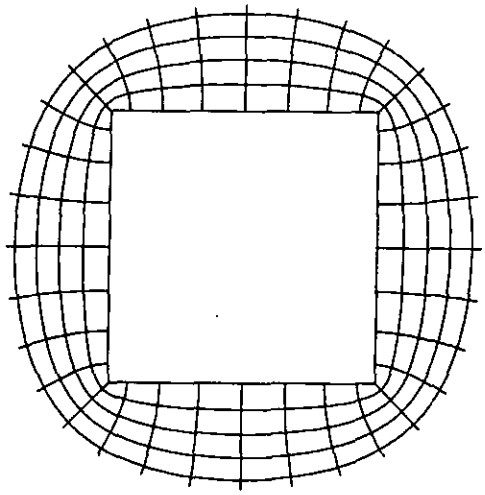

FIG. 14. Square using the inverse Timman method with $M = 150$, $N = 256$, $NP = 512$.

where

$$P(z) = \frac{1}{2\pi} \int_0^L \theta'(\tilde{\sigma}) \log(z - z(\tilde{\sigma}))\, d\tilde{\sigma},$$

γ is the capacity of the curve, as above, and ω is constant. Then

$$|f(z)| = \gamma^{-1} e^{|P(z)|}$$

and

$$|P(z(\sigma))| = \frac{1}{2\pi} \int_0^L \theta'(\tilde{\sigma}) \log |z(\sigma) - z(\tilde{\sigma})|\, d\tilde{\sigma}$$

can be approximated by subtracting out the logarithmic singularity as above. The error $|1 - |f(z)|\,|$ at a number of points on the boundary is listed in the tables.

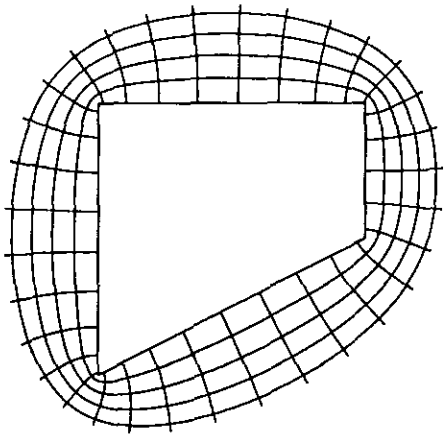

FIG. 15. Quadrilateral using the inverse Timman method with $M = 294$, $N = 512$, and $NP = 1024$.

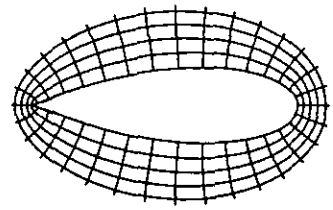

FIG. 16. Cosine airfoil using the inverse Timman method with $M = 60$, $N = 256$, and $NP = 512$.

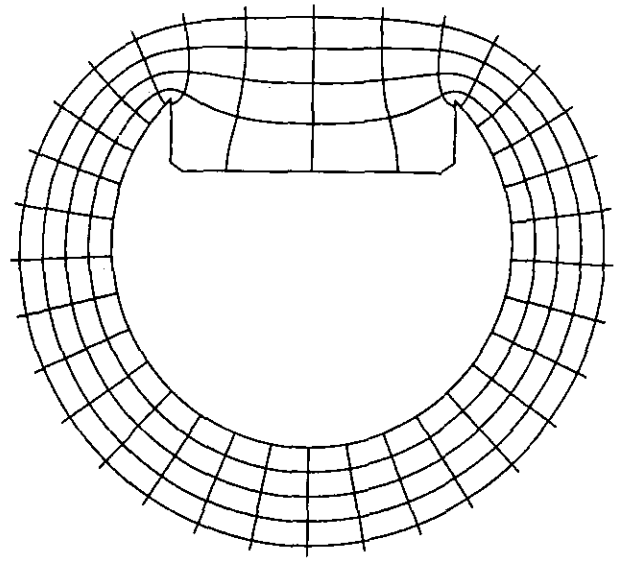

FIG. 17. Notched circle using the inverse Timman method with $M = 393$, $N = 512$, and $NP = 1024$.

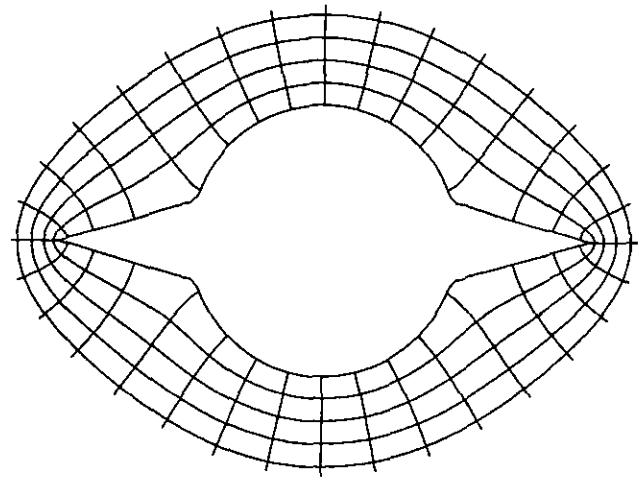

FIG. 18. Thick-wing body using the inverse Timman method with $M = 191$, $N = 256$, and $NP = 512$.

TABLE II

Discretization Errors for the Wing-Body Using the Inverse Timman Method (See Fig. 11)

M	$\lvert\theta-\theta_M\rvert$	N	$\lvert\sigma-\sigma_N\rvert$	$\lvert 1-\lvert f(z)\rvert\rvert$	CPU seconds (IBM ES9000)
104	0.15×10^{-1}	512	0.99×10^{-1}	0.16×10^{-1}	3.1
143	0.12×10^{-1}	512	0.72×10^{-1}	0.15×10^{-1}	6.9
200	0.96×10^{-2}	512	0.40×10^{-1}	0.78×10^{-2}	15.8
296	0.77×10^{-2}	512	0.27×10^{-1}	0.44×10^{-2}	31.5

EXAMPLE d (Wing-body, Fig. 11). The exact map for this region can be constructed by composing a Joukowski transformation and its inverse as given in [19]. The map is

$$z(w)=\frac{r_0}{2}(w+w^{-1})\pm\frac{1}{2}\sqrt{r_0^2(w+w^{-1})^2-4},$$

where the "body" is a circle of radius 1 centered at the origin, the "wing" is a slit of length s, and $r_0=\frac{1}{2}(s+1/s)$. In our example $s=1$. Table II gives the discretization errors.

Other examples where the exact map is not available are given in Fig. 12 through 18.

IV. SOME COMPARISON WITH OTHER METHODS

The method we have developed may be thought of as being related to the continuous Schwarz–Christoffel method developed in recent years by Davis and his coworkers; see [2, 9]. In that work an iteration for the complex boundary correspondence is made, based on quadratic interpolation of the tangent angle as a function of a parameter. This parameter is changed at each iteration in order to reduce the discrepancy between the target curve and the current iterate at the interpolation points. The iteration is one of successive approximation as is ours. Another common feature is that integrals with singularities due to corners can be dealt with with high accuracy. (See [12 or 13] for a discussion of Davis' method in the case of a polygon and for comparison of methods for handling the singularities in Schwarz–Christoffel integrals.) Our method differs in that our equation is for the boundary correspondence $\theta(\sigma)$ so that it is an inverse method to that of Davis. In a sense ours is closer to the idea of the Schwarz–Christoffel transformation, where the prevertices θ_k determine the map and are the essential parameters to determine in the numerical procedure; see [21].

Another recent work that should be mentioned in the context of piecewise smooth domains is that of Hough on the package CONFPACK [11]. The integral equation of Symm for the density in the single layer potential representation of $\log|dz/dw|$ is solved using collocation and orthogonal Jacobi polynomials on each smooth arc. In principle this method has the potential for high accuracy. The only pitfall we can see is the possibility of ill-conditioning of the full matrix equation that must be solved. The computations reported in [11] appear to be quite accurate, fast, and robust. Example 2 of [10] for the overlapping circles can be compared to our Table I. We point out that our method is $O(M^2)$, whereas CONFPACK is $O(M^3)$. Also, our method allows easily for an arbitrary number of corners. For instance, SCPACK [21] is $O(M^3)$ in the number of corners and slows down considerably for M greater than 20.

Combinations of explicit maps to remove corners with Fourier series methods have often been used; see [7]. (On the other hand, Ives [16] recommends against it.) The design of a general-purpose corner remover is a difficult task, however. Tracking the correct branch of the log, especially for slit regions like the wing-body, is tricky and the resulting smooth curve may be distorted. (This latter possibility could be avoided with the use of explicit Grassmann maps; see [8].) We have used a procedure in which we invert the region and rotate it about the image of the origin, successively removing each corner. An implementation of Fornberg's method [6] for periodic cubic spline boundaries is then used to map the interior of the smoothed region. However, this procedure is also sensitive to the positioning of the image of the origin inside the smooth region, and the tracking of branches for the fractional powers can be tricky if there are several corners. (For a problem like the wing-body a robust automatic procedure will be especially difficult to implement. Our experiments

TABLE III

Comparison of Three Methods for the Overlapping Circles with $\psi_1=1.8$ and $\psi_2=2.0$ (See Fig. 19)

Method	M	$\lvert\theta-\theta_M\rvert$	N	$\lvert\sigma-\sigma_N\rvert$	CPU seconds (IBM ES9000)
Inverse	46	0.41×10^{-2}	64	0.32×10^{-2}	0.8
Timman	97	0.25×10^{-2}	128	0.18×10^{-2}	2.3
	196	0.15×10^{-2}	256	0.95×10^{-3}	7.5
	298	0.11×10^{-2}	512	0.66×10^{-3}	16.4
Timman	—	—	128	0.97×10^{-3}	1.6
with	—	—	256	0.14×10^{-3}	3.0
corners	—	—	512	0.25×10^{-3}	5.8
Fornberg	—	—	128	0.23×10^{-2}	0.8
	—	—	256	0.67×10^{-3}	1.3
	—	—	512	0.35×10^{-3}	2.4
	—	—	1024	0.17×10^{-3}	4.6

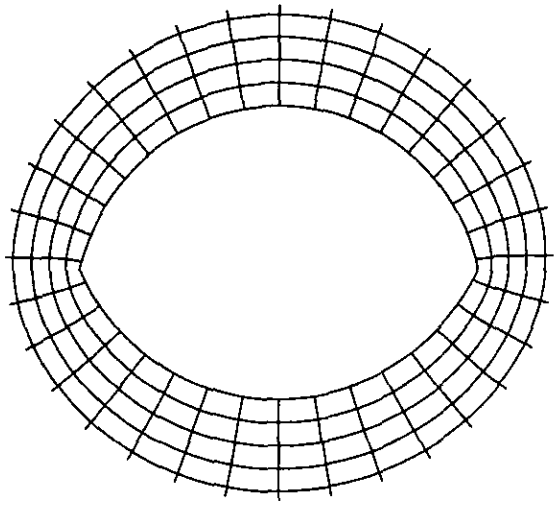

FIG. 19. Overlapping circles $\psi_1 = 1.8$ and $\psi_2 = 2.0$ for Table III.

indicate that a special branch of the logarithm with a polygonal branch line may be required.) If one is willing to apply corner removers on a case-by-case basis, we believe their combination with Fourier series methods has some appealing features. For regions which are not too extreme these $O(N \log N)$ methods are fast. For instance, the "thick-wing-body" in Fig. 18 required 3.7 CPU s with $N = 1024$ (successive iteration error of 0.13×10^{-4}) using corner removers and Fornberg's method, whereas our method took 45 CPU s with $M = 300$ (296) for 20 iterations and a successive iteration error of 0.13×10^{-6}. Rough checks of the discretization error indicate that it is about 10^{-4} for Fornberg's method and about 10^{-3} for ours. Similar levels of accuracy were observed in [4] for airfoils with a Karman–Trefftz transformation combined with Wegmann's method.

In Table III the inverse Timman method, Timman's method with corners, and Fornberg's method with corner removers are compared on the overlapping circles, Example c, with $\psi_1 = 1.8$ and $\psi_2 = 2.0$.

V. CONCLUDING REMARKS

The examples above show that the inverse Timman method, Timman's method with corners, and Fornberg's method are of comparable accuracy. The inverse Timman method is more robust in that it can handle regions with slits, sharp corners ($\alpha_k \pi < \pi$), and distorted geometries. The Fourier series methods are generally faster when applicable. However, Timman's method fails for regions with sharp corners, and Fornberg's method with corner removers will fail to converge if a good initial guess is not provided for the smoothed region. Also, a general-purpose corner-remover may be difficult to design.

REFERENCES

1. F. Bauer, P. Garabedian, D. Korn, and A. Jameson, *Supercritical Wing Sections II*, Lecture Notes in Econ. Math. Syst., Vol. 108 (Springer-Verlag, New York, 1975).
2. R. T. Davis, Paper No. 79-1463, AIAA 4th Computational Fluid Dynamics Conference, Williamsburg, VA, 1979.
3. T. K. DeLillo, *J. Comput. Appl. Math.* **19**, 363 (1987).
4. T. K. DeLillo and A. R. Elcrat, *SIAM J. Sci. Stat. Comput.* **12**, 399 (1991).
5. J. M. Floryan and C. Zemach, *J. Comput. Phys.* **72**, 347 (1987).
6. B. Fornberg, *SIAM J. Sci. Stat. Comput.* **1**, 386 (1980).
7. N. D. Halsey, *AIAA J.* **25**, 1286 (1987).
8. P. Henrici, *Applied and Computational Complex Analysis, Vol. III* (Wiley, New York, 1986).
9. M. Hoekstra, in *Numerical Grid Generation in Computational Fluid Dynamics*, edited by J. Häuser and C. Taylor (Pineridge Press, Swansea, UK, 1986), p. 59.
10. D. M. Hough, *J. Comput. Appl. Math.* **13**, 359 (1985).
11. D. M. Hough, IPS Research Report No. 90-11, ETH, Zürich, 1990 (unpublished).
12. L. H. Howell, Ph.D. dissertation, MIT, 1990.
13. L. H. Howell and L. N. Trefethen, *SIAM J. Sci. Stat. Comput.* **11**, 928 (1990).
14. M. K. Huang, in *Tenth International Conference on Numerical Methods in Fluid Dynamics*, Lecture Notes in Physics, Vol. 264 (Springer-Verlag, New York, 1986), p. 329.
15. M. K. Huang and C. Y. Chow, *J. Aircraft* **20**, 810 (1983).
16. D. C. Ives, in *Numerical Grid Generation*, edited by J. F. Thompson (North Holland, Amsterdam, 1982), p. 107.
17. A. Kaiser, Ph.D. dissertation, ETH, Zürich, 1986 (unpublished).
18. R. Menikoff and C. Zemach, *J. Comput. Phys.* **36**, 366 (1980).
19. J. N. Nielsen, *Missile Aerodynamics* (McGraw-Hill, New York, 1960), p. 27.
20. B. Noble, in *Nonlinear Integral Equations*, edited by P. Anselone (Univ. of Wisconsin Press, Madison, WI, 1964), p. 215.
21. L. N. Trefethen, *SIAM J. Sci. Stat. Comput.* **1**, 82 (1980).
22. L. C. Woods, *The Theory of Subsonic Plane Flow* (Cambridge Univ. Press, London, 1961).